

TOKAMARK: A Comprehensive Benchmark for MAST Tokamak Plasma Models

Cécile Rousseau
IBM Research Europe
Dublin, Ireland
rousseau.cecile@ibm.com

Nicola C. Amorisco
UK Atomic Energy Authority
Abingdon, UK
nicola.amorisco@ukaea.uk

Andrea Loreti
UK Atomic Energy Authority
Abingdon, UK
andrea.loreti@ukaea.uk

Adriano Agnello
STFC Hartree Centre
Daresbury, UK
adriano.agnello@stfc.ac.uk

Robert Akers
UK Atomic Energy Authority
Abingdon, UK
rob.akers@ukaea.uk

Samuel Jackson
UK Atomic Energy Authority
Abingdon, UK
samuel.jackson@ukaea.uk

Tobia Boschi
IBM Research Europe
Dublin, Ireland
tobia.boschi@ibm.com

Eszter Székely
UK Atomic Energy Authority
Abingdon, UK
eszter.szekely@ukaea.uk

Stanislas Pamela
UK Atomic Energy Authority
Abingdon, UK
Stanislas.Pamela@ukaea.uk

Juan Bernabe Moreno
IBM Research Europe
Dublin, Ireland
juan.bernabe-moreno@ibm.com

Mykhaylo Zayats
IBM Research Europe
Dublin, Ireland
mykhaylo.zayats1@ibm.com

Rodrigo H. Ordonez-Hurtado
IBM Research Europe
Dublin, Ireland
rodrigo.ordonez.hurtado@ibm.com

George K. Holt
STFC Hartree Centre
Daresbury, UK
george.holt@stfc.ac.uk

Alexander Whittle
UK Atomic Energy Authority
Abingdon, UK
alexander.whittle@ukaea.uk

Alessandra Pascale
IBM Research Europe
Dublin, Ireland
apascale@ie.ibm.com

Sue Thorne
STFC Hartree Centre
Daresbury, UK
sue.thorne@stfc.ac.uk

Abstract

Development and operation of commercially viable fusion energy reactors such as tokamaks require accurate predictions of plasma dynamics from sparse, noisy, and incomplete sensors readings. The complexity of the underlying physics and the heterogeneity of experimental data pose formidable challenges for conventional numerical methods, while simultaneously highlight the promise of modern data-native AI approaches. A major obstacle in realizing this potential is, however, the lack of curated, openly available datasets and standardized benchmarks. Existing fusion datasets are scarce, fragmented across institutions, facility-specific, and inconsistently annotated, which limits reproducibility and prevents a fair and scalable comparison of AI approaches. In this paper, we introduce **TOKAMARK**, a structured benchmark to evaluate AI models on real experimental data collected from the Mega Ampere Spherical Tokamak (MAST). TOKAMARK provides a comprehensive suite of tools designed to (i) unify access to multi-modal heterogeneous fusion data, and (ii) harmonize formats, metadata, temporal alignment and evaluation protocols to enable consistent cross-model and cross-task comparisons. The benchmark includes a curated list of 14 tasks spanning a range of physical mechanisms, exploiting a

variety of diagnostics and covering multiple operational use cases. A baseline model is provided to facilitate transparent comparison and validation within a unified framework. By establishing a unified benchmark for both the fusion and AI-for-science communities, TOKAMARK aims to accelerate progress in data-driven AI-based plasma modeling, contributing to the broader goal of achieving sustainable and stable fusion energy. The benchmark, documentation, and tooling will be fully open sourced upon acceptance to encourage community adoption and contribution.

CCS Concepts

- Applied computing → Physical sciences and engineering;
- Computing methodologies → Knowledge representation and reasoning;
- Software and its engineering → Software libraries and repositories; Open source model;
- Information systems → Extraction, transformation and loading.

Keywords

AI for science, Data-driven modeling, Fusion benchmark, Plasma dynamics, Multi-modal learning, MAST tokamak

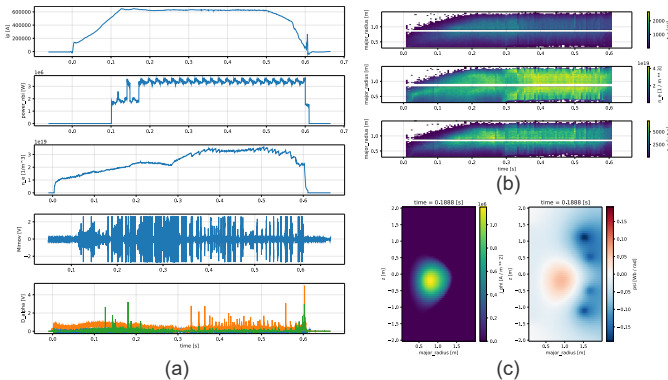


Figure 1: Examples of multi-modal signals from FAIR-MAST data: (a) time series of plasma current, line averaged density, NBI power, mirnov coils, and D_{α} signals; (b) Thomson scattering profiles of electron temperature, density, and pressure; (c) maps of plasma current and poloidal magnetic flux.

1 Introduction

Nuclear fusion power is being explored as a potential long-term energy source with a unique combination of benefits. It offers the prospect of a carbon-neutral energy supply with abundant fuel and significant safety advantages over nuclear fission. However, commercially viable fusion demands stable, sustained operation that produces more energy than the power plant consumes—a goal made difficult by the extreme physical conditions of thermonuclear confinement under which fusion must operate [13].

Magnetic confinement fusion reactors such as tokamaks aim to reproduce the process that powers the Sun in a controlled environment, confining a plasma hotter than 100 million degrees Celsius through the use of strong magnetic fields because no material surface can survive direct contact with such plasma [15, 44]. This environment forces all measurements to be non-invasive and indirect, only partially inferring plasma state while the underlying dynamics evolve on microsecond-to-millisecond timescales. In this work, we dedicate our attention to the problem of modeling fusion plasma dynamics in tokamaks—one of the central challenges in fusion research. This problem encompasses a wide set of predictive tasks, including plasma shape and equilibrium inference, transport and profile evolution, and forecasting of magnetohydrodynamics (MHD) activity and disruptions.

1.1 AI for fusion plasma modeling

Traditional approaches to tokamak plasma modeling are rooted in well-established first-principles descriptions of magnetized plasma dynamics. These descriptions are expressed through coupled, nonlinear systems of partial differential equations, whose numerical solutions often require high-fidelity, multi-scale simulations. While such models are indispensable for predictive studies, their computational cost severely limits their routine use, both in exploring the full phenomenology of plasma behavior, and in systematically interrogating large experimental datasets. In particular, many physically relevant regimes remain difficult to characterize in detail because comprehensive parameter scans and high-fidelity simulations are prohibitively expensive.

The same computational burden complicates data-driven inference. Key parameters governing plasma behavior—such as transport coefficients, source terms, or stability-relevant profile features—are frequently unmeasured or only indirectly observable, and inferring them typically requires repeated forward simulations embedded within optimization or system identification loops. As a result, fitting models to experimental data becomes costly and brittle across operating regimes. These limitations make the direct use of first-principles solvers infeasible for real-time applications, where stringent latency constraints rule out iterative or high-fidelity numerical solutions. The challenge is further compounded by the experimental characteristics of tokamak data.

Tokamaks deploy a broad suite of heterogeneous diagnostics—magnetics, optical and X-ray emission, microwave interferometry, and more [25]—mounted on or behind the reactor walls and engineered to withstand extreme heat, radiation, and electromagnetic stress. These sensors operate at widely different sampling rates, spatial resolutions, and noise characteristics, producing data that is inherently heterogeneous, incomplete, multi-rate, and noisy.

Together, the complexity of the underlying physics and the heterogeneity of the data create an opportunity where modern AI methods can provide significant advantages and complement physics-based modeling. Data-driven models are well suited to fusing multi-modal diagnostics, learning latent plasma representations, and capturing nonlinear, multi-scale temporal behavior without explicit physical parameterization. Unlike traditional solvers, AI models can operate directly on raw measurements, handle missing or asynchronous data, and produce accurate and efficient surrogates. However, these advantages come with caveats: learned models may fail silently when operating outside their training distribution, lack guaranteed physical consistency, and are generally more difficult to interpret.

Previous work applying AI to fusion plasma problems have demonstrated promising results across a variety of narrowly defined tasks, ranging from plasma shape reconstruction [29, 38, 40] and profile forecasting [1–3, 6, 20, 39, 41] to actuator optimization [2, 11, 26, 30, 32–34, 37, 42, 43, 45] and disruptions prediction [5, 8, 10, 14, 16, 19, 21, 23, 24, 27, 28, 47–50]. However, most of those efforts use bespoke pipelines tailored to a small set of diagnostics, single device and single scientific objective, relying heavily on task-specific feature engineering and handcrafted labeling procedures. While successful within their respective scopes, these approaches typically optimize models for individual tasks, which limits reuse across the experimental lifecycle. Adding to ongoing efforts [12, 46], more work is needed to move beyond isolated point solutions toward broad, interoperable models capable of understanding fusion plasmas in a comprehensive way.

Inspired by the success of Foundation Models (FM) in language and vision, there is a growing expectation that analogous models trained on large corpora of tokamak data could learn rich, transferable plasma representations [7]. These models aim to internalize latent physical structure directly from data, serving as data-driven analogs of first-principles knowledge that can support a wide range of downstream tasks. Although still in early stages, this paradigm suggests a path toward generalist AI systems for fusion that complement physics-based modeling and reduce the need for handcrafted pipelines [7].

Progress toward either specialized or generalist plasma models is hampered by the absence of open, standardized benchmarks. Fusion datasets remain fragmented across institutions, locked behind proprietary interfaces, or stored in domain-specific formats that are difficult for Machine Learning researchers to access or interpret [35]. Without unified task definitions, metrics, or evaluation protocols, it becomes impossible to provide a fair comparison of methods and to measure progress systematically. A benchmark is therefore needed to frame the plasma modeling problems in a broader and more structured way, enabling cross-comparison across algorithms, reproducibility across labs, and accessibility for researchers both inside and outside the fusion community.

At the same time, fusion diagnostic data provide a unique set of challenges going beyond those found in standard datasets from more established areas of AI. The data is inherently multi-modal, multi-rate, and multi-dimensional, with wide variations in signal quality, noise characteristics, and information content (see Figure 1 for an illustrative example). Many diagnostics operate asynchronously, contain gaps, or suffer partial failures; others produce high-dimensional structured outputs such as flux maps or spectrograms. This complexity demands dedicated modeling approaches that can handle missing data, fuse heterogeneous signals, different modalities, and reason across fast and slow timescales—capabilities that are difficult to stress-test without a standardized benchmark.

Taken together, these factors create a clear need for a comprehensive benchmark suite that defines common tasks, standardizes evaluation, and provides open access to representative fusion data. Establishing such a benchmark is essential for accelerating research, enabling fair comparison of models, and ultimately advancing data-driven plasma understanding and control.

1.2 TOKAMARK Benchmark Overview

To fill the need for comprehensive fusion plasma benchmarks, we introduce TOKAMARK, the first large, open benchmark for evaluating AI models trained on *real* fusion data.

Data. To the best of our knowledge, FAIR-MAST data represents the only openly available dataset of real tokamak diagnostics. Recent releases [17, 18] curate a collection of real experiments and corresponding diagnostics measurements from MAST tokamak. From FAIR-MAST, we select 39 signals across heterogeneous modalities, harmonize metadata and build standardized loaders.

Tasks. For TOKAMARK, we defined a diverse suite of 14 downstream tasks organized into 4 groups, designed to probe core capabilities required by AI models for fusion plasmas: (i) representation learning from heterogeneous diagnostics; (ii) temporal reasoning across fast and slow timescales; (iii) robustness to incomplete state information; and (iv) generalization across operating regimes. Rather than optimizing for a single downstream objective, the tasks span a cascade of physical processes—from fast magnetic response to slower, transport-driven evolution and long-horizon precursors of MHD activity—while remaining closely aligned with routine experimental workflows. Wherever possible, the tasks minimize reliance on expert-labeled targets, supporting self-supervised and weakly supervised formulations, and enabling systematic evaluation of transferable plasma representations.

Evaluation. We introduce a hierarchical evaluation protocol aligned with the structure of FAIR-MAST and with scientific objectives. This hierarchy assesses both low-level prediction quality and high-level scientific utility. For specialized models (single-task training), the hierarchy yields granular, signal-level diagnostics; for generalist models (FM-style pretrained and then fine-tuned across tasks), it provides modular comparisons across tasks and broad scientific objectives.

Baseline. Finally, we provide a strong yet accessible baseline: a *multi-branch convolutional encoder–decoder* architecture inspired by the previous works [31, 32] and largely expanded to ingest heterogeneous inputs and predict our task-specific targets. The architecture is trained independently for each task.

The following list summarizes our contributions:

- **Benchmark design.** We define 14 tasks organized into four groups, with a hierarchical evaluation protocol, standardized windowing, and error metrics.
- **Data packaging.** We freeze a stable subset of FAIR-MAST data, resolve schema inconsistencies, standardize metadata and units, and release it for reproducibility and long-time compatibility.
- **Tools and API.** We provide a Python package for task-specific data loading, processing and batching, masking and alignment utilities, and evaluation logic, integrated with the PyTorch stack.
- **Baseline models.** We release a multi-branch convolutional encoder–decoder baseline with reference configurations and training scripts, establishing reproducible baselines across all tasks.

2 Preliminaries

To ground TOKAMARK benchmark in the reality of complex heterogeneous fusion data, we first introduce a signal taxonomy that organizes these measurements by function and modality, which allows us to provide a consistent vocabulary for describing inputs, targets, and tasks in the benchmark.

2.1 Data Taxonomy

MAST is a spherical tokamak located in Culham, Oxfordshire (UK) and was operated by UKAEA and EURATOM from 1999 to 2013 [9, 22, 36]. MAST, and tokamaks in general, operates in short experimental cycles known as *discharges* or *shots*. The length of those cycles depends on the device size, and in the case of MAST typically last around 2–3 seconds. Over its operational lifetime, MAST produced more than 30,000 shots, with each shot containing diagnostic signals measuring various properties of the plasma, including the magnetic field, plasma temperature, shape parameters, and applied heating, to name a few. Recent works [17, 18] have created an open dataset of diagnostic data from a subset of the history of MAST. FAIR-MAST data contains 11,573 shots from the last five experimental campaigns on MAST. In this work, we utilized a total of 39 signals from FAIR-MAST data for the design of our benchmark tasks.

We organize all the selected signals along several complementary axes, as summarized in Table 1. First, we group signals by *category*,

Table 1: Signals taxonomy for TOKAMARK.

Category	Subcategory/Signals	Origin	Frequency	Modality
Magnetics	Flux loops, pickup coils; saddle coils	Diagnostic	5 kHz; 50 kHz	Profile
Kinetics	Thomson scattering; interferometer	Diagnostic	0.2 kHz; 4 kHz	Profile; time series
Radiatives	D _{alpha} , soft X-ray	Diagnostic	50 kHz	Profile
Fast magnetics	Mirnov coils	Diagnostic	500 kHz	Profile
Currents	Poloidal field coil currents; solenoid current, plasma current	Diagnostic	4 kHz	Profile; time series
Voltages	Poloidal field coil voltages	Actuator	4 kHz	Profile
References	Reference plasma current, reference plasma density	Actuator	4 kHz	Time series
Fueling	NBI power, gas puffing	Actuator	4 kHz	Time series
Equilibrium	Shape parameters, J_{tor} metrics; plasma boundary; flux map	Derived	0.2 kHz	Time series; profile; video

which encodes their physical semantics—that is, the physical quantities they represent and how they are used by MAST workflows. This information corresponds to the first two columns of Table 1. Note that the second column contains both individual signals and *subcategories*. These intermediate groupings are introduced for brevity: they consolidate multiple signals that are typically used together (at least within the proposed benchmark) and share the same structural and functional properties. For example, the *shape parameters* subcategory includes several attributes jointly describing plasma geometry. A full list of the signals used in this work is provided in the appendix in Table A.1.

Second, we distinguish signals by their *origin*, for which we define three classes: (i) **diagnostics**, corresponding to direct hardware measurements; (ii) **actuators**, representing controllable machine parameters used to steer plasma behavior; and (iii) **derived** signals, comprising quantities produced by reconstruction pipelines such as EFIT [4] (e.g., shape parameters or flux maps).

The third axis in Table 1 is *frequency*, reflecting the wide range of sampling rates across diagnostics, spanning from 0.2 kHz up to 500 kHz. Finally, the fourth axis is *modality*, describing the structural form of each signal: (i) **time series**, represented as 1D tensors (scalar value over time); (ii) **profiles**, represented as 2D tensors (vector over time); and (iii) **videos**, represented as 3D tensors (image over time). These latter two axes are particularly important for guiding the design of AI model architectures and loss functions.

2.2 Structural Taxonomy of Tasks

The downstream tasks in TOKAMARK share a common structural formulation designed to reflect the online, window-based nature of plasma control and forecasting in tokamak experiments. Rather than operating on full-shot signals (as is often done in offline post-discharge analysis), our tasks are defined using **input window** and **output window** anchored at a reference time point.

Each task consists of one or more *input signals*, and one or more *output signals* also referred to as targets. Inputs typically include both diagnostic signals (e.g., magnetics, radiatives, kinetics) and actuator signals (e.g., voltages, fueling), while outputs include either diagnostic signals or derived quantities like equilibrium reconstructions.

The alignment between the input and output windows naturally induces several families of modeling objectives:

- **Reconstruction.** Given a set of diagnostic signals A over the interval $[t_0 - \Delta_{\text{input}}, t_0]$, the goal is to reconstruct a related set of signals B over the *same* interval.
- **Autoregressive (AR) Forecasting.** Given diagnostic signals A over $[t_0 - \Delta_{\text{input}}, t_0]$ together with actuator trajectories over $[t_0 - \Delta_{\text{input}}, t_0 + \Delta_{\text{output}}]$, predict future values of the same diagnostic signals A over $[t_0, t_0 + \Delta_{\text{output}}]$.
- **Reconstructive (RC) Forecasting.** Using diagnostic signals A over $[t_0 - \Delta_{\text{input}}, t_0]$ and actuators over $[t_0 - \Delta_{\text{input}}, t_0 + \Delta_{\text{output}}]$, forecast a set of related outputs B over $[t_0, t_0 + \Delta_{\text{output}}]$ where B may contain signals as in A .

We further distinguish tasks by their temporal dependency structure: **Markovian** tasks require only a short input window to make forecasts, reflecting fast dynamics, whereas **Non-Markovian (NM)** tasks require substantially longer input histories even for short-term predictions.

2.3 Data-driven Challenges

To complete the description of FAIR-MAST data, we highlight three core data-centric challenges that AI systems must overcome in order to resolve tasks in TOKAMARK. These challenges arise directly from the heterogeneous, multi-instrument nature of tokamak diagnostics and the realities of operating large fusion experiments.

Multi-fidelity. Diagnostic systems operate at varying sampling rates, ranging from a few hundred hertz to several hundred kilohertz. Resampling to a common high-frequency time base is computationally expensive and often unnecessary, while down-sampling to the lowest frequency discards information critical for resolving fast plasma phenomena. Effective models must therefore integrate and represent multi-rate temporal data without losing fidelity.

Multi-modality. Signals differ not only in physical meaning, units, and numerical ranges, but also in structural forms of the corresponding data tensors. Their dimensionality can be from 1 to 3, with the number of channel in each non-temporal dimension varying from 1 up to 170. AI systems must be able to fuse these modalities into coherent representations suitable for downstream tasks.

Missing data. As with any experimental dataset, missing information is common. Entire signals may be absent for a given shot due to hardware issues. Individual signals may also contain missing time segments, for example due to limited acquisition windows or diagnostic failures. Naively discarding shots or windows with missing components wastes valuable examples and can introduce distributional bias. Robust approaches must therefore handle incomplete signals and irregular temporal coverage.

3 TOKAMARK: A MAST Benchmark

In this section, we provide a description of the main components of TOKAMARK: tasks, data preparation, and evaluation protocol.

3.1 Downstream Tasks

In TOKAMARK, we assembled a set of 14 tasks spanning across diverse timescales, modalities, and predictive objectives. We arranged them into 4 broad groups that represent some of the major modeling challenges arising in real-world fusion experiments. The 4 groups include: instantaneous reconstruction, short-term magnetics dynamics, slow transport-driven profile evolution, and long-range forecasting of rare but safety-critical events and MHD activity. Table 2 summarizes definitions of tasks and groups.

3.1.1 Group 1: Equilibrium Reconstruction. The tasks in Group 1 define a suite of reconstruction problems where the objective is to infer plasma equilibrium—its shape, boundaries, and various properties—from instantaneous magnetic measurements. The targets of the three tasks in this group span multiple modalities from scalar parameters (Task 1-1) to full plasma contour (Task 1-2) and two-dimensional representations of the poloidal magnetic flux (Task 1-3). The inputs of the tasks are identical and use magnetic diagnostics and actuator coil currents.

Equilibrium reconstruction is a foundational operation in tokamak experiments, performed routinely after every plasma discharge and forming the basis of essentially all downstream analysis. Traditionally, equilibrium is reconstructed by solving an inverse boundary-value problem governed by the Grad–Shafranov equation that describes the balance of magnetohydrodynamic force in axisymmetric plasmas. These solvers, like EFIT++ [4], require multiple iterations for convergence and rely on parameterized assumptions about plasma profiles, making it challenging to deploy them in real time.

Group 1 tasks evaluate whether AI models can infer equilibrium structure directly from raw diagnostics, providing fast, numerics-free surrogates that could underpin both offline interpretation and real-time control applications.

3.1.2 Group 2: Magnetics Dynamics. The tasks in Group 2 address short-timescale forecasting of magnetic signals, coil currents, and equilibrium evolution in response to applied actuator commands. Conceptually, these tasks parallel those in Group 1, but shift from static reconstruction to sequence-to-sequence forecasting with actuators signals now playing an essential role in the tasks inputs. Complexity increases in the three tasks in the group: from forecasting scalar quantities—such as plasma current evolution—to joint prediction of 2D equilibrium geometry over short horizons.

At these timescales, plasma evolution is dominated by inductive coupling between active coils, passive conducting structures, and

the plasma current, together with the local response of the equilibrium to perturbations. These dynamics govern how the plasma reacts to magnetic control actions during a discharge and are central to plasma position, shape, and current control. While these effects are routinely modeled offline, a model capable of achieving real-time latency would enable improved control policies.

Group 2 probes whether models can learn an effective description of the plasma response to the coupled magnetic dynamics of the active coils and vessel. This would directly target capabilities required for closed-loop control, scenario planning, and digital twin applications.

3.1.3 Group 3: Profile Dynamics. Group 3 tasks focus on modeling the temporal evolution of kinetic profiles—primarily, electron density and temperature—and on forecasting diagnostic signals associated with confinement-mode transitions. The three tasks in this group include short-horizon forecasting (Task 3-1 and Task 3-2) and pseudo-real-time reconstruction using partial, multi-rate diagnostic inputs (Task 3-3).

Profile evolution is governed by transport physics acting on particle and energy balance, introducing slower characteristic timescales and intrinsic memory effects compared to magnetic dynamics. These processes control energy confinement and overall plasma performance and are central to understanding transport, optimizing heating schemes, and predicting access to high-performance regimes. In practice, profile measurements are often sparse, delayed, or unavailable in real time.

The main goal of Group 3 tasks is to assess AI models’ ability to integrate incomplete diagnostic information over time to infer latent plasma state variables. This would support applications ranging from post-shot analysis, to integrated scenario design and real-time performance monitoring and control.

3.1.4 Group 4: MHD activity. Finally, the tasks in Group 4 comprise long-horizon forecasting of thermal quenches (Task 4-1 and Task 4-2), vertical displacement events (Task 4-3), current quenches (Task 4-4), and MHD activity leading to Locked Modes (Task 4-5). These tasks are focused on early detection of plasma instability and disruptions precursors that emerge across multiple diagnostic modalities. These tasks require processing of rich, high-frequency inputs—including magnetics, radiative diagnostics, and time-frequency MHD signatures—over extended temporal windows.

The onset of MHD instabilities and disruptions is tightly linked to the evolving equilibrium and current distribution, even when the nonlinear dynamics of the instability itself are difficult to model explicitly. Disruption avoidance and mitigation are critical operational requirements for present-day tokamaks and future reactors, directly affecting machine lifespan. In practice, early-warning systems rely on detecting subtle precursors distributed across multiple diagnostics and evolving over extended time windows.

Successful performance in Group 4 tasks would demonstrate the ability to integrate long-range temporal context and multi-modal information, allowing the models to anticipate loss-of-control events. This capabilities are essential for safe and reliable fusion operation.

3.1.5 Input and output window length. For fast magnetic and actuator dynamics (Group 2, tasks 3-1 and 3-2), the observed diagnostics provide a sufficient description of the system state, such that short

Table 2: Summary of groups and tasks for TOKAMARK.

	Task	Input Diagnostics	Input Actuators	Outputs	Type	Input Window	Output Window
Group 1	1-1	Magnetics, Currents	–	Shape parameters, J_{tor} metrics	Reconstruction	5 ms	5 ms
	1-2	Same as 1-1	–	Plasma boundary	Reconstruction	5 ms	5 ms
	1-3	Same as 1-1	–	Flux map	Reconstruction	5 ms	5 ms
Group 2	2-1	Magnetics, Currents	Voltages, NBI Power	Currents, J_{tor} metrics, Shape parameters	RC Forecasting	5 ms	25 ms
	2-2	Same as 2-1	Same as 2-1	Plasma boundary	RC Forecasting	5 ms	25 ms
	2-3	Same as 2-1	Same as 2-1	Flux map	RC Forecasting	5 ms	25 ms
Group 3	3-1	Thomson scattering	References, Fueling	Thomson scattering	AR Forecasting	5 ms	50 ms
	3-2	Thomson scattering, Radiatives	Same as 3-1	Radiatives	AR Forecasting	5 ms	50 ms
	3-3	Magnetics, Currents, Interferometer	Same as 3-1	Thomson scattering, J_{tor} metrics	RC Forecasting, NM history	5 ms	5 ms
Group 4	4-1	Magnetics, Mirnov coils, Currents, Radiatives, interferometer	References, Fueling	Soft X-ray	AR Forecasting, NM history	100 ms	
	4-2	Magnetics, Mirnov coils, Currents, Radiatives, Kinetics	Same as 4-1	Soft X-ray	AR Forecasting, NM history	100 ms	
	4-3	Same as 4-1	Same as 4-1	Shape parameters	RC Forecasting, NM history	100 ms	
	4-4	Same as 4-1	Same as 4-1	Plasma current	AR Forecasting, NM history	100 ms	
	4-5	Same as 4-1	Same as 4-1	Mirnov diagnostics	AR Forecasting, NM history	100 ms	

input windows are often adequate to predict near-term evolution. In contrast, profile evolution (*task 3-3*), confinement transitions, and MHD activity (Group 4) depend on latent plasma state variables—such as current and pressure profiles—that are only partially and indirectly observed. For these processes, accurate prediction requires integrating information over extended time intervals, making long input windows essential. By explicitly varying the temporal context required across tasks, the benchmark probes a model’s ability to learn both short-timescale system dynamics and long-range temporal dependencies arising from unobserved physics.

3.2 Data Preparation

We take all 11,573 available shots from FAIR-MAST data and extract the data for 39 signals required by our task definitions. Before being used for model training and evaluation, these signals undergo a standardized preprocessing pipeline to ensure consistent formatting and alignment.

Data split. The benchmark dataset is divided into disjoint *training*, *validation*, and *test* subsets. To avoid information leakage across sets, the split is performed at the shot level representing independent experiments, and employs random sampling technique. The split ratio used is 80%/10%/10%, and all hyperparameter tuning is conducted exclusively on the training and validation sets. The test set is held out and used only for the final performance evaluation.

Window segmentation. Shot-level signals data is segmented into input and output windows. The lengths of those windows are task-dependent as specified in Table 2. Windows are extracted using a sliding-window approach with a stride of 0.001 seconds

between consecutive windows. Each input window is paired with its corresponding output window and treated as an independent window-level sample. We note that signals are used at their original sampling rates, and no resampling or imputation is performed.

Handling of missing information. We impose additional constraints on the test set to ensure meaningful evaluation. Windows in which all input signals are entirely absent or composed solely of NaN values are excluded. Moreover, all output signals must be fully available over the entire prediction horizon.

3.3 Benchmark Evaluation

As part of TOKAMARK, we introduce a hierarchical evaluation protocol for assessing model performance which explicitly separates three levels of the hierarchy: (i) signals (individual physical quantities), (ii) tasks (well-defined scientific goals), and (iii) groups (broader physical objectives). This provides both, signal-level insights that help diagnose which physics regimes the model captures and higher-level scientific utility assessment.

To respect the hierarchy, the evaluation aggregates errors according to the following progression:

$$\text{samples} \rightarrow \text{windows} \rightarrow \text{signals} \rightarrow \text{tasks} \rightarrow \text{shots}.$$

Samples are the atomic level of data. For a given task and shot, each data sample is denoted as $y_{k,i,j}$ and corresponds to a particular sample j of the flattened data from window i and signal k . In the following, $y_{k,i,j}$ denotes the ground truth value and $\hat{y}_{k,i,j}$ the corresponding model prediction.

Windows are containers of the equal per-signal size storing N_k samples. We compute a window-level Root-Mean-Square error

(RMSE) error as:

$$\text{RMSE}_{k,i} = \sqrt{\frac{1}{N_k} \sum_{j=1}^{N_k} (y_{k,i,j} - \hat{y}_{k,i,j})^2} \quad (1)$$

For each **signal** k for a given task and shot and containing M_k windows, we aggregate all window errors via the single-shot signal RMSE and normalize it with the empirical standard deviation σ_k computed for signal k across all evaluation shots:

$$\text{RMSE}_k = \sqrt{\frac{1}{M_k} \sum_{i=1}^{M_k} \text{RMSE}_{k,i}^2}, \quad \text{NRMSE}_k = \frac{\text{RMSE}_k}{\sigma_k}, \quad (2)$$

which yields a dimensionless quantity that expresses prediction error relative to the natural variability of the target, making the metric comparable across signals. An error of $\text{NRMSE}_k = 1$ corresponds to a model no better than approximating the signal by its mean, while $\text{NRMSE}_k < 1$ indicates predictive value.

Concerning **tasks**, task-level errors \tilde{e}_t combine K_t normalized output signal errors into a single score using a uniform mean, allowing one to quantify model performance on the scientific objective as a whole:

$$\tilde{e}_t = \frac{1}{K_t} \sum_{k=1}^{K_t} \text{NRMSE}_k. \quad (3)$$

Shots represent independent experimental realizations, and therefore provide the final step of aggregation. We report signal-level and task-level errors as NRMSE based aggregated across shots quantities correspondingly defined as:

$$\text{Signal}_{\text{NRMSE}} = \frac{1}{S} \sum_{s=1}^S \text{NRMSE}_{k(s)}, \quad \text{Task}_{\text{NRMSE}} = \frac{1}{S} \sum_{s=1}^S \tilde{e}_{t(s)}. \quad (4)$$

Here, S is the total number of shots in the test set used for evaluation. Finally, the $\text{Group}_{\text{NRMSE}}$ score is taken as an average of the corresponding $\text{Task}_{\text{NRMSE}}$ scores.

4 Baseline Model Experiments

The baseline model is a multi-branch convolutional architecture designed to handle heterogeneous spatio-temporal inputs and outputs with varying dimensionalities (see Figure 2). Each input modality is processed by a dedicated encoder [31], and each target variable is generated by a corresponding decoder, all connected through a shared latent representation.

4.1 Model Description

Encoders. For each input variable $v_i \in (L_t^{(0,v_i)} \times L_h^{(0,v_i)} \times L_w^{(0,v_i)})$, an independent convolutional encoder is instantiated according to its modality: 1D convolutions for time series, 2D convolutions for profiles, and 3D convolutions for video signals. Each encoder consists of a stack of N convolutional layers with kernel size K , stride s , and padding p , followed by ReLU activations, max-pooling, and batch normalization. The feature maps are then flattened into a latent vector. The size of the feature map $L_d^{(\ell,v_i)}$ along dimension $d \in (t, h, w)$ after encoder layer $\ell \in [1, N]$ and the flattened latent

representation size $L^{(v_i)}$ for variable v_i can be computed as follows:

$$L_d^{(\ell,v_i)} = \left\lceil \frac{1}{2} \left\lceil \frac{L_d^{(\ell-1,v_i)} + 2p - K}{s} \right\rceil + p - \frac{1}{2} \right\rceil + 1, \quad (5)$$

$$L^{(v_i)} = 2^{N-1} D L_t^{(N,v_i)} L_h^{(N,v_i)} L_w^{(N,v_i)}. \quad (6)$$

Latent fusion backbone. The latent embeddings produced by all encoder branches are concatenated and passed through a shared backbone. This backbone consists of a sequence of linear layers, each followed by ReLU activation and dropout, progressively reducing the dimensionality back to D . This shared representation provides a compact summary of all input data and connects the encoder and decoder blocks.

Decoders. For each output variable $v_o \in (L_t^{(N,v_o)} \times L_h^{(N,v_o)} \times L_w^{(N,v_o)})$, the decoder branch reconstructs the target output from the latent vector, mirroring the encoder structure. The shared latent vector is first reshaped into a compressed feature map of dimensionality $L^{(v_o)}$, which is then progressively upsampled using transposed convolutions with the output padding o_p . Cropping operations are applied after each transposed convolution to ensure that the reconstructed outputs exactly match the required target dimensions $L_d^{(\ell,v_o)}$. The sizes $L_d^{(\ell,v_o)}$ of the feature map before decoder layer $\ell \in [0, N-1]$ and $L^{(v_o)}$ of the compressed flattened feature map are:

$$L_d^{(\ell,v_o)} = \left\lceil s \cdot (L_d^{(\ell+1,v_o)} - 1) - 2p + K + o_p \right\rceil, \quad (7)$$

$$L^{(v_o)} = 2^{N-1} D L_t^{(0,v_o)} L_h^{(0,v_o)} L_w^{(0,v_o)}. \quad (8)$$

4.2 Experimental Settings

Parameter Settings. For our architecture, we adopt a latent embedding dimension of $D = 16$, with $N = 3$ convolutional layers per encoder and decoder blocks. Each convolution uses a kernel size $K = 3$, stride $s = 3$, padding $p = 1$, and output padding $o_p = 1$. The same architectural hyperparameters—number of layers, kernel size, stride, and padding—are applied consistently across all tasks.

Data Preprocessing. We run a set of model-specific preprocessing: first, we replace NaN values with zeros, and then we standardize data using signal-computed zero mean and unit variance scaler. This ensures numerical stability and helps to improve training convergence. The training and validation data is downsampled by taking samples with a stride of 0.005 seconds for Markovian tasks, and 0.025 seconds for non-Markovian tasks. Furthermore, because our architecture requires a fixed-length context, inputs for non-Markovian tasks are truncated to a duration of 50 ms.

Training Procedure. We train our model on mini-batches containing data from 32 shots using the Adam optimizer with a learning rate of 1×10^{-4} and early stopping with a patience of 10 epochs. We also employ a multi-output mean squared error loss, which averages the loss across all outputs of the model. Table 3 summarizes models sizes per each task.

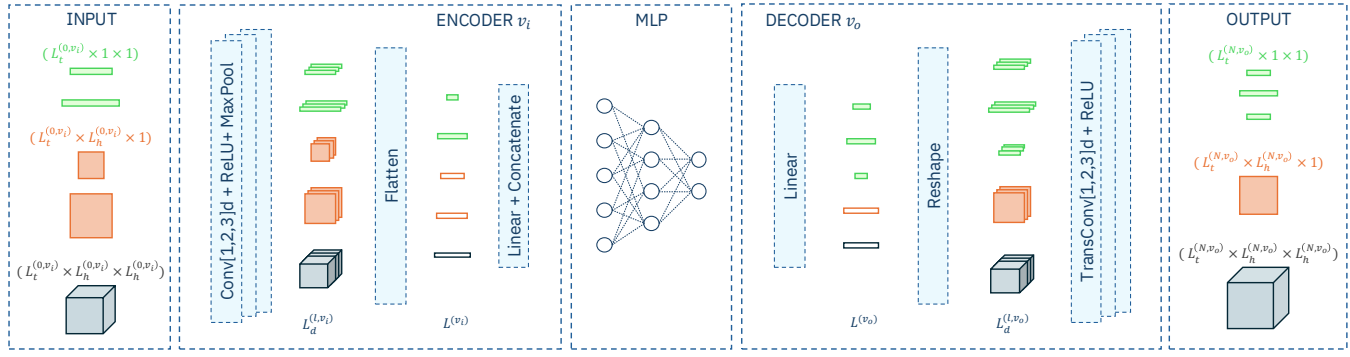


Figure 2: Multi-branch convolutional encoder–decoder.

4.3 Experimental Results

The results of the baseline model evaluation on TOKAMARK tasks are presented in Table 3. Those results demonstrate a clear distinction between tasks complexities: the model performs well for equilibrium reconstruction (Group 1) and magnetics dynamics (Group 2) tasks with the group-level scores below 0.17, but degrades for profile dynamics (Group 3) and MHD activities (Group 4) tasks, confirming these are more difficult tasks. Notably, even within the same group, tasks scores vary substantially. For instance, plasma boundary reconstruction and forecasting tasks Task 1-2 and Task 2-2 are resolved much better than their counterparts within the respective groups. On the other side, the error score for Task 4-5 is by far the worst and exceeds unity, suggesting the corresponding signals are poorly constrained or inadequately represented. Finally, we provide signal level error metrics in the appendix in Table A.2.

These results should be interpreted with a consideration to the nature of a baseline model: the architecture is generic, without physics-informed priors or task-specific tuning. The scores reported—especially those for profile dynamics and MHD activity tasks—highlight intrinsic benchmark difficulty rather than flaws in optimization. Nevertheless, this baseline establishes a realistic lower bound and identifies areas for improvement.

5 Conclusions

In this work, we introduced TOKAMARK, the first large-scale, open benchmark specifically designed for evaluating AI models on MAST tokamak diagnostics. We provided a complete open-source training and evaluation stack for 14 diverse downstream tasks together with a strong baseline model, creating an integrated framework for benchmarking, tooling, and model development.

TOKAMARK opens the door to more systematic and reproducible research in fusion plasma modeling. It provides a platform for exploring advanced representation learning of plasma, short- and long-horizon predictions, and generalization across tokamak operating regimes. We believe the adoption of TOKAMARK will accelerate progress toward practical, data-driven fusion models, foster stronger collaboration between the fusion and machine learning communities, and ultimately contribute to the development of stable and commercially viable fusion energy.

Table 3: Task and Group errors for TOKAMARK tasks.

Task/Group	NRMSE	Parameters(M)
Task 1-1	0.1882	0.343
Task 1-2	0.0482	0.239
Task 1-3	0.2552	0.257
<i>Group 1</i>	0.163	-
Task 2-1	0.1551	0.436
Task 2-2	0.0517	0.277
Task 2-3	0.1724	0.295
<i>Group 2</i>	0.1264	-
Task 3-1	0.3252	0.158
Task 3-2	0.3309	0.761
Task 3-3	0.3607	0.336
<i>Group 3</i>	0.3389	-
Task 4-1	0.3445	1.518
Task 4-2	0.3311	1.571
Task 4-3	0.2702	0.672
Task 4-4	0.4292	0.687
Task 4-5	1.0053	4.741
<i>Group 4</i>	0.4761	-

References

- [1] J. Abbate, R. Conlin, and E. Kolemen. 2021. Data-driven profile prediction for DIII-D. *Nuclear Fusion* 61, 4 (March 2021), 046027. doi:10.1088/1741-4326/abe08d Publisher: IOP Publishing.
- [2] Joseph Abbate, Rory Conlin, Ricardo Shousha, Keith Erickson, and Egemen Kolemen. 2023. A general infrastructure for data-driven control design and implementation in tokamaks. *Journal of Plasma Physics* 89, 1 (Feb. 2023), 895890102. doi:10.1017/S002377822001040
- [3] J. Abbate, E. Fable, G. Tardini, R. Fischer, E. Kolemen, and the ASDEX Upgrade Team. 2025. Combining physics-based and data-driven models for quantitatively accurate plasma profile prediction that extrapolates well; with application to DIII-D, AUG, and ITER tokamaks. *Nuclear Fusion* 65, 5 (April 2025), 056014. doi:10.1088/1741-4326/adc283 Publisher: IOP Publishing.
- [4] L.C. Appel and I. Lupelli. 2018. Equilibrium reconstruction in an iron core tokamak using a deterministic magnetisation model. *Computer Physics Communications* 223 (2018), 1–17. doi:10.1016/j.cpc.2017.09.016
- [5] Enrico Aymerich, Giuliana Sias, Fabio Pisano, Barbara Cannas, Sara Carcangiu, Carlo Sozzi, Chris Stuart, PJ Carvalho, Alessandra Fanni, and JET Contributors. 2022. Disruption prediction at JET through deep convolutional neural networks using spatiotemporal information from plasma profiles. *Nuclear Fusion* 62, 6 (2022), 066005.
- [6] Ian Char, Youngseog Chung, Joseph Abbate, Egemen Kolemen, and Jeff Schneider. 2024. Full Shot Predictions for the DIII-D Tokamak via Deep Recurrent Networks. <http://arxiv.org/abs/2404.12416> arXiv:2404.12416 [physics].
- [7] R Michael Churchill. 2025. AI foundation models for experimental fusion tasks. *Frontiers in Physics* 12 (2025), 153134.
- [8] R. M. Churchill, B. Tobias, Y. Zhu, and DIII-D team. 2020. Deep convolutional neural networks for multi-scale time-series classification and application to

tokamak disruption prediction using raw, high temporal resolution diagnostic data. *Physics of Plasmas* 27, 6 (June 2020), 062510. doi:10.1063/1.5144458

[9] GF Counsell, RJ Akers, Lynton C Appel, D Applegate, KB Axon, Y Baranov, C Brickleay, C Bunting, RJ Butterly, PG Carolan, et al. 2005. Overview of MAST results. *Nuclear fusion* 45, 10 (2005), S157.

[10] PC De Vries, MF Johnson, B Alper, P Buratti, TC Hender, HR Koslowski, V Riccardo, Jet-Efda Contributors, et al. 2011. Survey of disruption causes at JET. *Nuclear fusion* 51, 5 (2011), 053018.

[11] Jonas Degrave, Federico Felici, Jonas Buchli, Michael Neunert, Brendan Tracey, Francesco Carpanese, Timo Ewalds, Roland Hafner, Abbas Abdolmaleki, Diego de las Casas, Craig Donner, Leslie Fritz, Cristian Galperti, Andrea Huber, James Keeling, Maria Tsimpoukelli, Jackie Kay, Antoine Merle, Jean-Marc Moret, Séb Noury, Federico Pesamosca, David Pfau, Olivier Sauter, Cristian Sommariva, Stefano Coda, Basil Duval, Ambrogio Fasoli, Pushmeet Kohli, Koray Kavukcuoglu, Demis Hassabis, and Martin Riedmiller. 2022. Magnetic control of tokamak plasmas through deep reinforcement learning. *Nature* 602, 7897 (Feb. 2022), 414–419. doi:10.1038/s41586-021-04301-9 Number: 7897 Publisher: Nature Publishing Group.

[12] Qianyun Dong, Zhengwei Chen, Rongpeng Li, Zongyu Yang, Feng Gao, Yihang Chen, Fan Xia, Wulyu Zhong, and Zifeng Zhao. 2025. Adapted Swin Transformer-based real-time plasma shape detection and control in HL-3. *Nuclear Fusion* 65, 2 (jan 2025), 026031. doi:10.1088/1741-4326/ada2fe

[13] AJH Donné, M Cox, N Sauthoff, and K Schoenberg. 2025. Beyond power gain: Toward a comprehensive milestone framework for all fusion energy concepts. *Physics of Plasmas* 32, 9 (2025).

[14] Diogo R. Ferreira, Pedro J. Carvalho, and Horácio Fernandes. 2020. Deep Learning for Plasma Tomography and Disruption Prediction from Bolometer Data. *IEEE Transactions on Plasma Science* 48, 1 (Jan. 2020), 36–45. doi:10.1109/TPS.2019.2947304 arXiv:1910.13257 [physics].

[15] Jeffrey P. Freidberg. 2007. *Plasma Physics and Fusion Energy*. Cambridge University Press.

[16] B H Guo, D L Chen, B Shen, C Rea, R S Granetz, L Zeng, W H Hu, J P Qian, Y W Sun, and B J Xiao. 2021. Disruption prediction on EAST tokamak using a deep learning algorithm. *Plasma Physics and Controlled Fusion* 63, 11 (Sept. 2021), 115007. doi:10.1088/1361-6587/ac228b Publisher: IOP Publishing.

[17] Samuel Jackson, Saiful Khan, Nathan Cummings, James Hodson, Shaun de Witt, Stanislas Pamela, Rob Akers, and Jeyan Thiyanagalingam. 2025. An Open Data Service for Supporting Research in Machine Learning on Tokamak Data. *IEEE Transactions on Plasma Science* (2025). doi:10.1109/TPS.2025.3583419

[18] Samuel Jackson, Saiful Khan, Nathan Cummings, James Hodson, Shaun de Witt, Stanislas Pamela, Rob Akers, Jeyan Thiyanagalingam, and The MAST Team. 2024. FAIR-MAST: A fusion device data management system. *SoftwareX* 27 (2024), 101869.

[19] Julian Kates-Harbeck, Alexey Svyatkovskiy, and William Tang. 2019. Predicting disruptive instabilities in controlled fusion plasmas through deep learning. *Nature* 568, 7753 (April 2019), 526–531. doi:10.1038/s41586-019-1116-4 Number: 7753 Publisher: Nature Publishing Group.

[20] A. Kit, A. E. Järvinen, Y. R. J. Poels, S. Wiesen, V. Menkovski, R. Fischer, M. Dunne, and ASDEX-Upgrade Team. 2024. On learning latent dynamics of the AUG plasma state. *Physics of Plasmas* 31, 3 (March 2024), 032504. doi:10.1063/5.0174128 arXiv:2308.14556 [physics].

[21] Spangher Lucas, Matteo Bonotto, William Arnold, Dhruba Chayapathy, Tommaso Gallignani, Alexander Spangher, Francesco Cannarile, Daniele Bigoni, Eliana De Marchi, and Cristina Rea. 2024. DisruptionBench: A robust benchmarking framework for machine learning-driven disruption prediction. doi:10.21203/rs.3.rs-4245117/v1

[22] Hendrik Meyer, RJ Akers, F Alladio, Lynton C Appel, KB Axon, N Ben Ayed, P Boerner, RJ Butterly, PG Carolan, D Ceric, et al. 2009. Overview of physics results from MAST. *Nuclear fusion* 49, 10 (2009), 104017.

[23] Kevin J. Montes. 2021. *Interpretable Machine Learning for Prediction and Avoidance of Disruptions in Tokamak Plasmas*. Thesis. Massachusetts Institute of Technology. <https://dspace.mit.edu/handle/1721.1/142684> Accepted: 2022-05-24T19:18:44Z.

[24] K. J. Montes, C. Rea, R. A. Tinguely, R. Sweeney, J. Zhu, and R. S. Granetz. 2021. A semi-supervised machine learning detector for physics events in tokamak discharges. *Nuclear Fusion* 61, 2 (Jan. 2021), 026022. doi:10.1088/1741-4326/abcd9 Publisher: IOP Publishing.

[25] A.W. Morris and the MAST team. 2002. Diagnostic Developments for the Mast Spherical Tokamak. *Advanced Diagnostics for Magnetic and Inertial Fusion*. Springer, Boston, MA. (2002). doi:10.1007/978-1-4419-8696-2_68

[26] David Orozco, Brian Sammuli, Jayson Barr, William Wehner, and David Humphreys. 2022. Neural Network-Based Confinement Mode Prediction for Real-Time Disruption Avoidance. *IEEE Transactions on Plasma Science* 50, 11 (Nov. 2022), 4157–4164. doi:10.1109/TPS.2022.3198596 Conference Name: IEEE Transactions on Plasma Science.

[27] M. Priyanka, J. Sangeetha, and C. Jayakumar. 2024. A Review of Traditional and Data-Driven Approaches for Disruption Prediction in Different Tokamaks. *E3S Web of Conferences* 477 (2024), 00039. doi:10.1051/e3sconf/202447700039

[28] C. Rea, R. S. Granetz, K. Montes, R. A. Tinguely, N. Eidietis, J. M. Hanson, and B. Sammuli. 2018. Disruption prediction investigations using Machine Learning tools on DIII-D and Alcator C-Mod. *Plasma Physics and Controlled Fusion* 60, 8 (June 2018), 084004. doi:10.1088/1361-6587/aac7fe Publisher: IOP Publishing.

[29] Riccardo Rossi, Michela Gelfusa, Andrea Murari, and on behalf of JET contributors. 2023. On the potential of physics-informed neural networks to solve inverse problems in tokamaks. *Nuclear Fusion* 63, 12 (Nov. 2023), 126059. doi:10.1088/1741-4326/ad067c Publisher: IOP Publishing.

[30] Raphael Schramm, Alexander Bock, Emiliano Fable, Joerg Stober, Marc Maraschek, Maximilian Reisner, Rainer Fischer, and Hartmut Zohm. 2024. Development and application of a predictive model for advanced tokamak scenario design. *Nuclear Fusion* (Jan. 2024). doi:10.1088/1741-4326/ad2062

[31] Jaemin Seo, Rory Conlin, Andrew Rothstein, SangKyeun Kim, Joseph Abbate, Azarakhsh Jalalvand, and Egemen Kolemen. 2023. Multimodal prediction of tearing instabilities in a tokamak. In *2023 International Joint Conference on Neural Networks (IJCNN)*. IEEE, 1–8.

[32] Jaemin Seo, SangKyeun Kim, Azarakhsh Jalalvand, Rory Conlin, Andrew Rothstein, Joseph Abbate, Keith Erickson, Josiah Wai, Ricardo Shousha, and Egemen Kolemen. 2024. Avoiding fusion plasma tearing instability with deep reinforcement learning. *Nature* 626, 8000 (2024), 746–751.

[33] Jaemin Seo, Y.-S. Na, B. Kim, C. Y. Lee, M. S. Park, S. J. Park, and Y. H. Lee. 2021. Feedforward beta control in the KSTAR tokamak by deep reinforcement learning. *Nuclear Fusion* 61, 10 (Sept. 2021), 106010. doi:10.1088/1741-4326/ac121b Publisher: IOP Publishing.

[34] J. Seo, Y.-S. Na, B. Kim, C. Y. Lee, M. S. Park, S. J. Park, and Y. H. Lee. 2022. Development of an operation trajectory design algorithm for control of multiple 0D parameters using deep reinforcement learning in KSTAR. *Nuclear Fusion* 62, 8 (July 2022), 086049. doi:10.1088/1741-4326/ac79be Publisher: IOP Publishing.

[35] P Strand, DP Coster, M Plocieniak, S de Witt, IA Klampans, J Decker, F Imbeaux, JF Artaud, B Bosak, N Cummings, et al. 2022. A FAIR based approach to data sharing in Europe. *Plasma Physics and Controlled Fusion* 64, 10 (2022), 104001.

[36] A Sykes, RJ Akers, LC Appel, ER Arends, PG Carolan, NJ Conway, GF Counsell, G Cunningham, A Dnestrovskij, Yu N Dnestrovskij, et al. 2001. First results from MAST. *Nuclear Fusion* 41, 10 (2001), 1423.

[37] J. Vega, A. Murari, S. Dormido-Canto, G. A. Rattá, and M. Gelfusa. 2022. Disruption prediction with artificial intelligence techniques in tokamak plasmas. *Nature Physics* 18, 7 (July 2022), 741–750. doi:10.1038/s41567-022-01602-2 Number: 7 Publisher: Nature Publishing Group.

[38] J. T. Wai, M. D. Boyer, and E. Kolemen. 2022. Neural net modeling of equilibria in NSTX-U. *Nuclear Fusion* 62, 8 (July 2022), 086042. doi:10.1088/1741-4326/ac77e6 Publisher: IOP Publishing.

[39] T. Wakatsuki, M. Yoshida, E. Narita, T. Suzuki, and N. Hayashi. 2023. Simultaneous control of safety factor profile and normalized beta for JT-60SA using reinforcement learning. *Nuclear Fusion* 63, 7 (May 2023), 076017. doi:10.1088/1741-4326/acd393 Publisher: IOP Publishing.

[40] Chenguang Wan, Zhi Yu, Alessandro Pau, Olivier Sauter, Xiaojuan Liu, Qiping Yuan, and Jiangang Li. 2023. A machine-learning-based tool for last closed-flux surface reconstruction on tokamaks. *Nuclear Fusion* 63, 5 (April 2023), 056019. doi:10.1088/1741-4326/acbfcc Publisher: IOP Publishing.

[41] Chenguang Wan, Zhi Yu, Feng Wang, Xiaojuan Liu, and Jiangang Li. 2021. Experiment data-driven modeling of tokamak discharge in EAST. *Nuclear Fusion* 61, 6 (April 2021), 066015. doi:10.1088/1741-4326/abf419 Publisher: IOP Publishing.

[42] Allen M. Wang, Alessandro Pau, Cristina Rea, Oswin So, Charles Dawson, Olivier Sauter, Mark D. Boyer, Anna Vu, Cristian Galperti, Chuchu Fan, Antoine Merle, Yoeri Poels, Cristina Venturini, Stefano Marchioni, and the TCV Team. 2025. Learning Plasma Dynamics and Robust Rampdown Trajectories with Predict-First Experiments at TCV. doi:10.48550/arXiv.2502.12327 arXiv:2502.12327 [physics].

[43] Allen M. Wang, Oswin So, Charles Dawson, Darren T. Garnier, Cristina Rea, and Chuchu Fan. 2024. Active Disruption Avoidance and Trajectory Design for Tokamak Ramp-downs with Neural Differential Equations and Reinforcement Learning. (2024). doi:10.48550/ARXIV.2402.09387 Publisher: arXiv Version Number: 1.

[44] J Wesson. 1987. *Tokamaks*. Oxford University Press, New York, NY. <https://www.osti.gov/biblio/5589784>

[45] Bin Yang, Zhenxing Liu, Xianmin Song, Xiangwen Li, and Yan Li. 2020. Modeling of the HL-2A plasma vertical displacement control system based on deep learning and its controller design. *Plasma Physics and Controlled Fusion* 62, 7 (May 2020), 075004. doi:10.1088/1361-6587/ab8a64 Publisher: IOP Publishing.

[46] Zongyu Yang, Zhenghao Yang, Wenjing Tian, Jiyuan Li, Xiang Sun, Guohui Zheng, Songfei Liu, Nianmin Wu, Rongpeng Li, Zhaohe Xu, Bo Li, Zhongbing Shi, Zhe Gao, Wei Chen, Xiaoquan Ji, Min Xu, and Wuluyu Zhong. 2025. FusionMAE: large-scale pretrained model to optimize and simplify diagnostic and control of fusion plasma. arXiv:2509.12945 [physics.plasm-ph] <https://arxiv.org/abs/2509.12945>

[47] Ming Zhang, Qiqi Wu, Wei Zheng, Yangxing Shang, and Yuxing Wang. 2020. A database for developing machine learning based disruption predictors. *Fusion Engineering and Design* 160 (Nov. 2020), 111981. doi:10.1016/j.fusengdes.2020.111981

- [48] Jinxiang Zhu, Cristina Rea, Robert S Granetz, Earl S Marmar, Kevin J Montes, Ryan Sweeney, Roy A Tinguely, DL Chen, Biao Shen, BJ Xiao, et al. 2021. Scenario adaptive disruption prediction study for next generation burning-plasma tokamaks. *Nuclear Fusion* 61, 11 (2021), 114005.
- [49] JX Zhu, Cristina Rea, Kevin Montes, RS Granetz, Ryan Sweeney, and Roy Alexander Tinguely. 2021. Hybrid deep-learning architecture for general disruption prediction across multiple tokamaks. *Nuclear Fusion* 61, 2 (2021), 026007.
- [50] J. X. Zhu, C. Rea, R. S. Granetz, E. S. Marmar, R. Sweeney, K. Montes, and R. A. Tinguely. 2023. Integrated deep learning framework for unstable event identification and disruption prediction of tokamak plasmas. *Nuclear Fusion* 63, 4 (March 2023), 046009. doi:10.1088/1741-4326/acb803 Publisher: IOP Publishing.

A Full Set of Signals

Table A.1 presents the complete set of signals used in TOKAMARK. The table is aligned with the taxonomy in Table 1 and specifies signals within each category and subcategory. We note, that both the data used by TOKAMARK as well as the FAIR-MAST data are stored in per-shot *zarr* files. Within each *zarr* file, signals are organized into groups (which are similar, though not identical, to the categories listed in Table A.1). We therefore provide each signal's full identifier in the format "group name"- "signal name".

B Signal Level Errors

In addition to the task- and group-level errors we also report more granular signal-level errors in Table A.2. Moreover, that table includes not only NRMSE-based signal errors but also RMSE-, MAE- and NMAE-based errors, all computed analogously.

Table A.1: Full set of signals used in TokAMARK.

Category	Subcategory/Signals	Full signal name
Magnetics	Flux loops	magnetics-flux_loop_flux
	Pickup coils	magnetics-[b_field_pol_probe_ccbv_field, b_field_pol_probe_obb_field, b_field_pol_probe_obb_field]
	Saddle coils	magnetics-b_field_tor_probe_saddle_voltage
Kinetics	Thomson scattering	thomson_scattering-[t_e, n_e]
	Interferometer	interferometer-n_e_line
Radiatives	D_alpha	spectrometer_visible-filter_spectrometer_dalpha_voltage
	soft X-ray	soft_x_rays-[horizontal_cam_lower, horizontal_cam_upper]
Fast magnetics	Mirnov coils	magnetics-[b_field_tor_probe_cc_field, b_field_pol_probe_omv_voltage]
Currents	Poloidal field coil currents	pf_active-[coil_current, solenoid_current]
	Plasma current	summary-ip
Voltages	Poloidal field coil voltages	pf_active-coil_voltage
References	Reference plasma current	pulse_schedule-i_plasma
	Reference plasma density	pulse_schedule-n_e_line
Fueling	NBI power	summary-power_nbi
	Gas puffing	gas_injection-total_injected
Equilibrium	Shape parameters	equilibrium-[elongation, elongation_axis, triangularity_upper, triangularity_lower, x_point_r, x_point_z, minor_radius, magnetic_axis_r, magnetic_axis_z]
	J _{tor} metrics	equilibrium-[q95, beta_tor, beta_pol, beta_normal, bvac_rmag, bphi_rmag]
	plasma boundary	equilibrium-[lcfs_r, lcfs_z]
	flux map	equilibrium-psi

Table A.2: Signal errors across all tasks and groups.

Task	Full signal name	Signal _{RMSE}	Signal _{MAE}	Signal _{NRMSE}	Signal _{NMAE}
Group 1	equilibrium-beta_normal	0.3686	0.2664	0.2734	0.1976
	equilibrium-beta_pol	0.0870	0.0609	0.2668	0.1868
	equilibrium-beta_tor	0.8385	0.6512	0.2415	0.1876
	equilibrium-bphi_rmag	0.0293	0.0251	0.1497	0.1281
	equilibrium-bvac_rmag	0.0230	0.0213	0.1367	0.1270
	equilibrium-elongation	0.0501	0.0414	0.2342	0.1936
	equilibrium-elongation_axis	0.0564	0.0472	0.2676	0.2240
	equilibrium-magnetic_axis_r	0.0147	0.0117	0.1557	0.1237
	equilibrium-magnetic_axis_z	0.0105	0.0086	0.1429	0.1173
	equilibrium-minor_radius	0.0114	0.0091	0.1805	0.1437
	equilibrium-q95	0.5950	0.4729	0.1749	0.1390
	equilibrium-triangularity_lower	0.0223	0.0181	0.2277	0.1851
	equilibrium-triangularity_upper	0.0220	0.0178	0.2155	0.1744
	equilibrium-x_point_r	0.1099	0.0799	0.1431	0.1041
1-1	equilibrium-x_point_z	0.0926	0.0599	0.0130	0.0084
	equilibrium-lcfs_r	0.0211	0.0147	0.0559	0.0390
	equilibrium-lcfs_z	0.0262	0.0197	0.0404	0.0303
1-3	equilibrium-psi	0.0142	0.0050	0.2552	0.0901
Group 2	equilibrium-beta_normal	0.3102	0.2210	0.2301	0.1639
	equilibrium-beta_pol	0.0734	0.0509	0.2252	0.1562
	equilibrium-beta_tor	0.7493	0.5718	0.2158	0.1647
	equilibrium-bphi_rmag	0.0225	0.0178	0.1152	0.0911
	equilibrium-bvac_rmag	0.0181	0.0163	0.1079	0.0969
	equilibrium-elongation	0.0460	0.0373	0.2147	0.1742
	equilibrium-elongation_axis	0.0533	0.0441	0.2527	0.2090
	equilibrium-magnetic_axis_r	0.0138	0.0109	0.1462	0.1155
	equilibrium-magnetic_axis_z	0.0102	0.0079	0.1393	0.1080
	equilibrium-minor_radius	0.0106	0.0084	0.1677	0.1324
	equilibrium-q95	0.5151	0.4151	0.1514	0.1220
	equilibrium-triangularity_lower	0.0214	0.0170	0.2187	0.1734
	equilibrium-triangularity_upper	0.0214	0.0168	0.2093	0.1641
	equilibrium-x_point_r	0.0976	0.0656	0.1272	0.0854
	equilibrium-x_point_z	0.0870	0.0557	0.0122	0.0078
	pf_active-coil_current	535.13	374.30	0.1057	0.0739
	pf_active-solenoid_current	913.93	749.73	0.0726	0.0595
	summary-ip	26035.74	21395.01	0.0803	0.0660
2-2	equilibrium-lcfs_r	0.0212	0.0149	0.0561	0.0393
2-2	equilibrium-lcfs_z	0.0307	0.0230	0.0473	0.0355
2-3	equilibrium-psi	0.0096	0.0037	0.1724	0.0663
Group 3	thomson_scattering-n_e	4.73×10^{18}	3.43×10^{18}	0.3307	0.2399
	thomson_scattering-t_e	107.00	71.96	0.3196	0.2149
	soft_x_rays-horizontal_cam_lower	0.00719	0.00343	0.2382	0.1136
	soft_x_rays-horizontal_cam_upper	0.00735	0.00355	0.2717	0.1313
	spectrometer_visible-filter_spectrometer_dalpha_voltage	0.2172	0.1226	0.4830	0.2726
Group 4	equilibrium-beta_normal	0.4389	0.2981	0.3256	0.2211
	equilibrium-beta_pol	0.0987	0.0628	0.3028	0.1926
	equilibrium-beta_tor	0.9948	0.7296	0.2865	0.2101
	thomson_scattering-n_e	7.35×10^{18}	5.69×10^{18}	0.5143	0.3984
	thomson_scattering-t_e	125.35	94.33	0.3744	0.2817
4-1	soft_x_rays-horizontal_cam_lower	0.00962	0.00523	0.3184	0.1731
4-1	soft_x_rays-horizontal_cam_upper	0.01003	0.00562	0.3705	0.2077
4-2	soft_x_rays-horizontal_cam_lower	0.00971	0.00488	0.3215	0.1616
4-2	soft_x_rays-horizontal_cam_upper	0.00922	0.00485	0.3406	0.1792
4-3	equilibrium-magnetic_axis_z	0.0198	0.0171	0.2702	0.2341
4-4	summary-ip	139237.10	91351.51	0.4292	0.2816
4-5	magnetics-b_field_pol_probe_omv_voltage	0.1595	0.0683	0.9371	0.4014
4-5	magnetics-b_field_tor_probe_cc_field	2.15×10^{-5}	5.95×10^{-6}	1.0734	0.2972